Astron. Astrophys. 70, 769—775 (1978)

ASTRONOMY
AND
ASTROPHYSICS

H II Regions and CO Clouds: The Blister Model

F. P. Israel*
Owens Valley Radio Observatory, California Institute of Technology 102–24, Pasadena, California 91125, USA

Received December 12, 1977, revised March 17, 1978

Summary. A comparison of H II region and CO cloud observations shows that the majority of H II regions are located at the edges of molecular clouds, and have structure suggestive of ionization fronts surrounded by less dense envelopes. The bulk of the ionized material streams away from the associated molecular cloud. The general applicability of this blister model has important consequences for models of both H II region evolution and star formation.

Key words: H II regions — CO clouds — blister model — star formation

I. Introduction

Surveys of CO emission in the direction of galactic H II regions (Liszt, 1973; Wilson et al., 1974; Blair et al., 1975) show that most H II regions are closely associated with molecular clouds. The (CO) clouds or cloud complexes almost always have much larger dimensions than the nearby H II regions.

What exactly is the relation between an H II region and its associated CO cloud? Particularly interesting is a recent suggestion by several authors, that at least to specific H II regions a picture applies in which the exciting star is located near the edge of a neutral cloud. The star causes ionization fronts to move slowly into the cloud. A cavity filled with ionized gas and dust may result, from which gas flows away into space. Since the whole situation is very reminiscent of a blister on the skin of a molecular cloud, I will in the following refer to it as the blister model. The question now arises to what extent the blister model is generally applicable to galactic H II region.

The question of the structure of H II regions may be pursued by studying a small number of regions in great detail and by explaining their individual characteristics (case studies) or by studying the overall properties of a much larger sample of H II regions and explaining their common characteristics (statistical studies). The first approach has largely been followed by optical observers, notably the groups in Manchester and Marseille. In this Paper I will follow the second approach. Part of my discussion will be based on a sample of about 60 galactic H II regions, observed with the Westerbork Synthesis Radio Telescope—WSRT—(Israel et al., 1973—Paper I; Israel, 1976a and b—Papers II and III; Israel, 1977a and b—Papers IV and IV; Felli et al., 1977—Paper V; Deharveng et al., 1976; Harten, 1976, and Matthews et al., 1977). In order to enlarge the sample of H II regions for which CO velocities are available, I also observed CO emission in the direction of 15 Sharpless (1959) H II regions with the Texas millimeter telescope.

These observations are described first in Sect. II. Sect. III then reviews those H II regions to which case studies (mainly at optical wavelengths) have shown the blister model to be applicable; Sect. IV discusses the relative positions of H II regions and CO clouds; Sect. V presents notes on the radio morphology of H II regions; Sect. VI compares the radial velocities of H II regions and their associated CO clouds, and Sect. VII lists the conclusions drawn.

II. CO Observations

All observations were made with the 5 m antenna of the Millimeter Wave Observatory (MWO) at Fort Davis, Texas[1] in May 1976. The receiver was operated in the frequency switching mode; the SSB system temperature varied from 1200–1500 K during the observations. Velocity coverage and resolution at the 115.3 GHz frequency of $^{12}C^{16}O$ were 26 km s^{-1} and 0.65 km s^{-1} re-

* Part of this work was done while the author was at the Sterrenwacht, Leiden, Netherlands

[1] The Millimeter Wave Observatory is operated by the Electrical Engineering Research Laboratory of the University of Texas at Austin, with support from the National Aeronautics and Space Administration, the National Science Foundation, and McDonald Observatory.

Table 1. CO in the direction of Sharpless H II regions

Name	Central Position α(1950.0)	δ(1950.0)	Optical[a] Size (arc min)		T_A^* (K)	V_{LSR} (km s^{-1})	
(1)	(2)	(3)	(4)	(5)	(6)	(7)	(8)
S 48	$18^h19^m30^s$	-14°38'00"	15x12	3.0	3.0(0,0)	+52.6	+52.6
				8.5	9.0(0,-5)	+46.3	+45.0
S 57	18 27 30	-08 39 00	2x2	<1.2	4.5(0,+5)	-	+36.6
S 71	18 59 30	-02 05 00	2x1	<0.9	<0.9	(+35)	-
S 82	19 28 15	+18 10 00	10x10	3.9	20.5(0,+5)	+24.8	+24.2
S 84	19 46 45	+18 16 00	15x3	1.6	1.7(0,+5)	+28.6	+28.3
S 104	20 15 45	+36 35 00	7x7	2.5	6.3(+5,0)	+ 2.8	+ 1.5
S 112	20 33 00	+45 20 00	13x13	1.7	3.1(0,+5)	-12.2	-12.0
S 125	21 51 20	+47 00 00	10x10	4.1	26.2(+5,0)	+ 7.5	+ 7.8
S 128	21 30 20	+55 38 00	1x1	2.0	2.6(0,+5)	-73.7	-74.3
S 135	22 20 18	+58 28 00	22x15	3.4	8.0(0,+5)	-20.8	-20.8
S 139	22 20 15	+58 28 00	10x7	2.1	8.6(0,+5)	-21.4	-22.0
				1.3	2.2(0,+5)	-15.2	-14.8
S 142[b]	22 46 00	+57 52 00	25x20	9.8	-	-41.0	-
S 144	22 42 35	+59 38 00	10x7	2.2	2.5(0,+5)	+ 1.2	+ 0.6
				2.2	2.4(-5,0)	- 6.7	- 4.6
S 157[b]	23 14 00	+59 45 30	3x3	15.0	-	-42.8	-
S 159[b]	23 13 30	+60 50 30	7x7	20.0	-	-56.0	-
				6.9	-	-53.8	-

[a] From Lynds (1965)
[b] Region was fully mapped

spectively. The line intensities are given in terms of T_A^*, defined as the antenna temperature corrected for all antenna and atmospheric losses. Calibration was done using the standard chopping-wheel technique. I estimate the errors in the velocity to be about 1 km s^{-1}, somewhat larger than usual for this system because of a small drift in the synthesizer frequency during the observations.

For all except three H II regions (S 142, S 157, and S 159) I observed the CO emission from only five points: at a central position coinciding with the H II region, and at positions 5′ north, south, east, and west of this. The results of these observations are given in Table 1. Col. 1 lists the name of the region Col. 2 and 3 the observed central position and Col. 4 the optical size of the H II region. Col. 5 gives the antenna temperature T_A^* detected at the central position, and Col. 6 the highest T_A^* among the five positions. The numbers in parentheses identify that position: the first refer to east (+) or west (−), the second to south (−) or north (+). Col. 7 and 8 list the radial velocities corresponding to the antenna temperatures in the two preceding columns. The CO clouds near S 142, S 157, and S 159 were mapped in both ^{12}CO and ^{13}CO; the results will be presented in a later paper. The central positions given here are those of peak T_A^*.

III. The Structure of Individual H II Regions

Optical studies of radial velocities and radio observations of various molecular lines in the Orion nebula led Zuckerman (1973) to propose a structure in which the Orion nebula consists of ionized gas streaming away from an associated molecular cloud. He was the first to work out a blister-type model, but apparently the time was ripe for the idea, since independently from each other, Balick et al. (1974) and Dopita et al. (1974) also proposed similar models for the Orion nebula, while Grasdalen (1974) arrived at comparable conclusions about the structure of NGC 2024 (Orion B). It was realized at the time that an attractive consequence of the blister model, at least for Orion, is that it solves the apparent age discrepancy between the Trapezium stars and the H II region. The dense ionized core is continuously replenished by matter streaming through the ionization front. Thus it can survive for a much longer time than indicated by its expansion age.

In the case of the Orion nebula, further support for the blister model was furnished by the identification and study of ionization fronts (Dopita et al., 1974, 1975; Elliott and Meaburn, 1974a and b). The same authors also found similar structures in the Hour Glass region of M 8 (see also Elliott and Meaburn, 1975b). It is of interest to note that the ionization fronts are also clearly shown as bright ridges in the high resolution radio map of Orion A by Martin and Gull (1975). Further optical observations show the relevance of blister-type models to IC 1318 (Goudis and Meaburn, 1974), M 17 (first proposed by Gull and Balick, 1974, but studied in much greater detail by Elliott and Meaburn, 1975a, and Meaburn, 1975a), S 206 (Deharveng et al., 1976) and the extragalactic H II region 30 Dor in the Large Magellanic Cloud (Elliott et al., 1977). A good review of optical observations and their interpretations in terms of H II region structure is given by Meaburn (1975b).

A curious feature of almost all optically-studied H II regions is the observed splitting of spectral lines in several places (see e.g. Wilson et al., 1959; Deharveng, 1973; Dopita et al., 1975 for Orion A; Elliott and Meaburn, 1975b, for M 8; Goudis and Meaburn, 1976 for M 17, M 8, and M 16). Meaburn (1977) has presented an extensive review of the phenomenon. A small splitting (indicating motions up to 20–40 km s^{-1}) can be taken to represent different flows of ionized gas and thus supports the blister model. The origin of large scale motions (cf. Meaburn, 1977) is more obscure. It should be mentioned however, that only a small fraction of the total ionized mass appears to be involved. In general most of the emission takes place at velocities close to the average velocity.

Mainly because of a difference in angular resolution (typically 1″ versus 10–300″) optical observations tend to reveal much more complicated structures than radio observations. The effect of several disturbing factors is particularly notable in the optical studies. Ionization fronts may be irregularly shaped, reflecting density inhomogeneities in the neutral cloud; this may give rise

Table 2. Location of H II regions with respect to CO clouds

Name	Distance to Nearest CO peak r (pc)	Mean Radius of CO Maximum $\bar{R}$ (pc)	Ratio $r/\bar{R}$	Size of HII Region d (pc)	References
(1)	(2)	(3)	(4)	(5)	(6)
G45.46	5.3	7	0.8	3.3	1, 2
G45.47	3.0	7	0.4	0.1	1, 2
G45.48	12.7	2.5	4.4	0.7	1, 2
S90	2.0	2.5	0.8	1.5	3, 4
G69.54	2.9	3	1.0	0.1	5, 2
S99	2.6	3.0	0.9	1.8	5, 6
W58A	6.5	6.5	1.0	0.2 (0.8)	5, 6
W58B	4.9	6.5	0.8	1.3	5, 6
W58C	1.3	6.5	0.2	0.2 (1.6)	5, 6
W58D	7.8	6.5	1.2	1.8	5, 6
G75.77	4.3	4.1	1.1	1.3	1, 2
G75.78	6.0	4.1	1.5	0.1	1, 2
G75.84	2.3	4.2	0.6	0.5	1, 2
G75.84	2.0	4.2	0.5	1.0	1, 2
S125	1.9	3.5	0.6	1.8	5, 4
S140	0.8	0.8	1.0	0.5	7
S142	1.4	1.2	1.2	(16)	5, 4
G110.25	0.2	1.0	0.2	0.5	3, 8
S156	0.8	2.5	0.3	1.5	3, 8
S157A	2.5	2.2	1.1	1.3	5, 8
S157B	2.0	2.2	0.9	0.1	5, 8
S158A,B	1.7	4.0	0.4	2.5	9, 8
S158G	1.3	5.0	0.3	0.1	9, 8
S159	1.0	1.5	0.7	0.1 (3.0)	9, 8
S184	2.3	2.3	1.0	5.0	5, 4
S206	3.3	3.5	0.9	4.3 (54)	3, 10
S228	1.0	1.1	0.9	1.4 (2.6)	11, 4
S235	0.3	5.5	0.1	4.0	3, 12
S235A	1.1	4.5	0.2	0.2	3, 12
S235C	1.2	4.5	0.3	0.9	3, 12
S254	0.6	1.0	0.6	3.2	3, 13
S255	0.8	0.7	1.1	0.8	3, 13
G192.58	0.5	0.7	0.7	0.1	3, 13
G256	0.6	0.7	0.9	0.3	3, 13
S257	0.7	0.7	1.0	0.7	3, 13

References to Table 2

1. Baud (1977)
2. Matthews et al. (1977)
3. Blair et al. (1975)
4. Paper VI
5. Israel, to be published
6. Paper II
7. Blair et al. (1977)
8. Paper I; Paper IV
9. Dickel, priv. communication
10. Deharveng et al. (1976)
11. Lucas and Encrenaz (1975)
12. Israel and Felli (1977)
13. Paper III

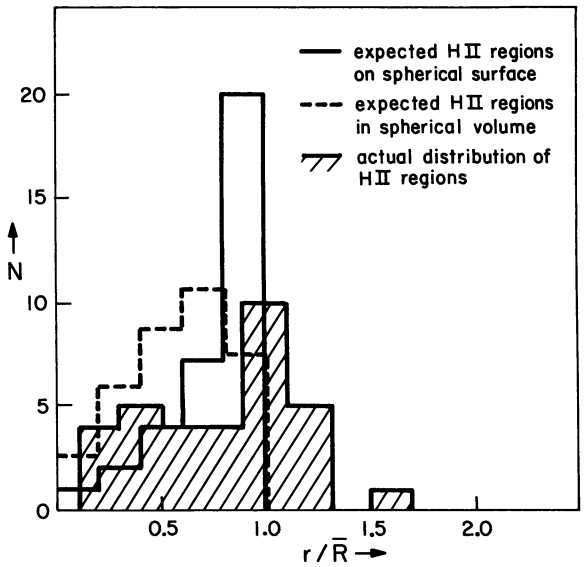

Fig. 1. Actual and expected distributions of H II regions with respect to CO clouds. See text

to ionized gas streams in different directions. The densest parts of the neutral cloud may survive in the H II regions for a considerable time as partially ionized globules (Dyson, 1973; Tenorio-Tagle, 1977). The effects of these are studied, for instance by Dopita et al. (1974). Stellar mass loss and stellar winds may play a significant role (Dyson, 1977a). Some of their effects are, for instance, visible in S 162 (Icke, 1973) and S 206 (Dyson, 1977b).

The conclusion to be drawn from this section is that several well-studied H II regions show complicated detailed structures, that however fit well into the framework of the blister model. To what extent a majority of galactic H II regions show overall properties characteristic of the blister model will be discussed in the following sections.

IV. Relative Positions of H II and CO Peaks

Previously, I suggested that the W 58 complex and the S 156/G 110.25 group are situated at the edge of their associated neutral clouds (Papers II and IV). Indeed this appears to be the case for most H II regions, as is clear from a comparison of the radio positions of H II regions with those of the nearby CO clouds.

In Table 2 I list those H II regions (both optically visible and observed) that are associated with a charted CO cloud and for which high-resolution WSRT maps exist. Col. 1 gives the name of the H II region, Col. 2 gives the projected linear distance r between the H II radio peak and the nearest CO peak; Col. 3 gives the mean linear (half power) radius $\bar{R}$ of the CO maximum; Col. 4 lists the ratio $r/\bar{R}$ and Col. 5 gives the linear size of the H II region. References to the CO (first number) and radio continuum (second number) maps are given in Col. 6. In some cases, the CO radius may be affected by resolution effects. Also, a ratio $r/R>1$ does not necessarily mean that the H II region and the CO cloud are not in contact; this also depends on the size of the H II region and the actual shape of the CO cloud.

Of the 32 listed H II regions, all except G 45.48 appear to be related to a CO peak. G 45.48 is however within the boundaries of an extended CO cloud (see Baud, 1977). Excluding this object the average value $\bar{r}$ between the brightness peak of an H II region and the nearest CO peak is 2.3 ± 1.9 pc, while the $\bar{R}$ of the associated CO maximum (cloud) is 2.9 ± 1.9 pc. The average ratio $\overline{r/R}$ is 0.79 ± 0.41.

This result is closer to the expected value $\overline{r/R}=0.87$ for H II regions randomly distributed over the surfaces of spherical CO clouds than to the value $\overline{r/R}=0.52$ expected for H II regions randomly distributed throughout the volume of spherical CO clouds. The actual distribution of the H II regions from Table 2 over the different values of $r/\bar{R}$ is compared to the two expected distributions in Fig. 1. Although not excellent (due to the idealized assumptions made—especially the assumption of spherical symmetry of the CO cloud), there is clearly a better agreement between the observed distribution and that expected for H II regions on the surfaces of CO clouds than that expected for H II regions inside CO clouds; very clear examples listed in Table 2 are S 140,

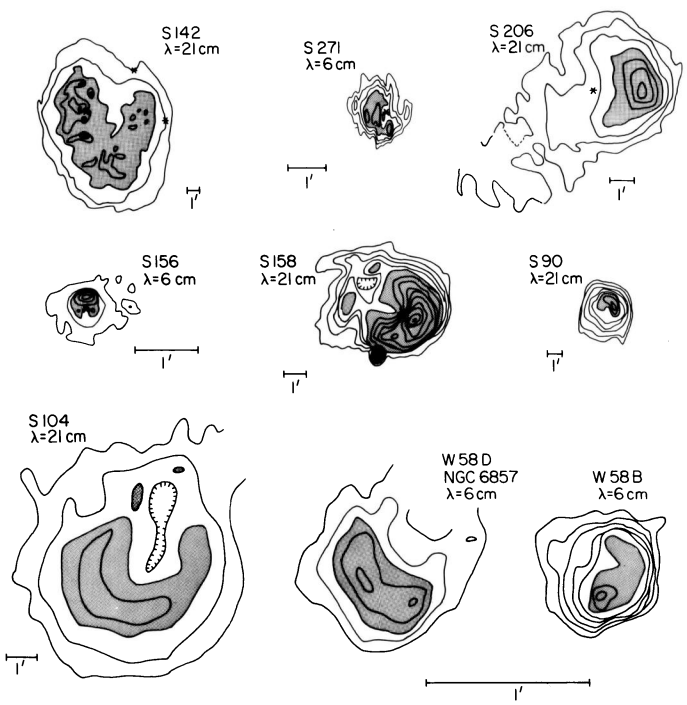

Fig. 2. Radio structure of several H II regions, taken from Papers I, II, III, IV, and VI. S 156, W 58 B, W 58 D, and S 271 are on a linear scale three times larger than that of S 90, S 158, and S 206; S 142 is on a linear scale two times smaller

S 206 and S 228. Thus the average space distance of H II region maxima to the nearest CO peaks is about 3 pc, and the H II regions are probably located at or near the edge of their associated CO clouds.

V. Remarks on The Radio Morphology of H II Regions

I will search the roughly 60 H II region maps obtained with the WSRT for those structural details that are characteristic of the blister model, such as the presence of cores and envelopes, and of forms like curved ridges or incomplete shells. Core/envelope structure is defined as one in which the increase of radio surface brightness towards the brightness peak of the region is not gradual, but shows a clear discontinuity in the gradient, so that the H II region appears to consist of one or more relatively small and bright peaks, surrounded by a larger, less intense envelope.

Characteristics of a core/envelope source are: a) a difference in of an order of magnitude peak surface brightness between core and envelope of an b) a difference in size between the two factor two to five. Consequently there is a difference in r.m.s. electron density of about an order of magnitude. Although cores and envelopes can be of any class, the cores are predominantly high-density, compact objects ($n_e > 10^3$ cm^{-3}; $d < 0.5$ pc).

Several H II regions that I did not consider as core/envelope sources nevertheless show a brightness distribution that might be regarded as indicative of a weak core-envelope structure. Examples are S 157 A (Paper I, IV), S 271 (Paper III), S 142, and S 184 (Paper V, VI). In these cases, the difference in surface brightness between suspected core and envelope, and the change in surface brightness are too small to be certain of their nature. I note that these are all fairly diffuse, medium density objects ($n_e \sim 100$–1000 cm^{-3}). In the detection of shell or ridgelike structure, sufficient resolution is a more critical factor than in the search for core/envelope structure. For that reason, all objects in the WSRT sample that show such structure are extended, well resolved H II regions. Observations with the higher resolution Cambridge 5 km Telescope have, however, shown that shell structure also exists in several compact H II regions such as K 3–50, S 157 B, S 158 Gl, and S 159 A (Wynn-Williams, private communication).

Of the compact objects, about half show a core/envelope structure; in the remaining cases the angular resolution was insufficient to conclude anything about their structure. A large proportion of the core/envelope sources also show curved ridges or incomplete shells. There are about ten sources that show ridges or shells, but that do not clearly show a core/envelope division. It is of interest to note that seven out of nineteen (40%) of the well resolved medium density H II regions show little or no (i.e. very low contrast) structure in their radio maps. In the case of the low density H II regions this is true for ten out of seventeen (60%) regions. Good examples of such featureless H II regions are S 125 (Paper VI) and S 254 (Paper II).

Thus the WSRT maps of galactic H II regions indicate that in most cases, H II regions consist of high density ridges (almost certainly ionization fronts) surrounded by less dense, more extended diffuse envelopes. Generally, the envelopes have flux densities equal to, or greater than the core components. It therefore seems that the extended, featureless H II regions have progressed so far on their evolutionary path that most density and surface brightness contrasts that were originally present have now been washed out.

VI. Relative Velocities of H II Regions and CO Clouds

Blister type models predict a difference in the mean velocity of an H II region and the velocity of the associated CO cloud. H II regions that are optically visible are supposedly located on the near side of their molecular cloud. Therefore, a more negative velocity is expected for the H II region than for the CO cloud—a prediction first made by Zuckerman (1973). Indeed, Liszt (1973), Wilson et al. (1974), and Blair et al. (1975) thought to find such an effect in their observations. In all these cases the sample was too small to do more than note a trend. Moreover, often the Hα line velocity rather than the H 109α radio recombination line velocity was taken for the mean velocity of the ionized gas. The

mean velocity as derived from Hα observations can be severely in error, especially given observed dispersions of 10–15 km s^{-1} in H II regions. In particular, the Hα velocity is not necessarily representative of the mean velocity of an H II region as it can be strongly influenced by irregular extinction across the nebula and by incorrect weighting of individual data points in the case of Fabry-Perot observations. For individual comparisons radio recombination line velocities are thus preferable. Given a large enough sample, the Hα velocities can be used, albeit with caution, since the average velocity difference appears to be small. For nineteen H II regions (see Table 3) I found $\Delta V(\mathrm{H}\,109\alpha - \mathrm{H}\alpha) = +0.1 \pm 0.5$ km s^{-1}. In the following, I will use H 109α recombination line velocities whenever available, Hα velocities in the remainder of cases.

In the case of obscured H II regions this problem does obviously not exist, but here it is not immediately clear what to expect. If the majority of these regions are obscured by unrelated foreground clouds, I expect roughly equal numbers of H II regions to be on the near and on the far side of the associated cloud, so that on average the velocity difference between H II region and cloud will be zero. If on the other hand the majority are obscured by their associated clouds, this means that they are located on the far side of their clouds. Therefore I expect a positive velocity difference in that case. As will be shown later, the former appears to be the case in the available sample of obscured H II regions.

In Table 3 I list all relevant velocity data from the literature and from Table 1. Fig. 3 shows that the result of a comparison of the H 109α/Hα velocities of H II regions with the CO velocities of their associated clouds. On average, the visible H II regions show a blueshift of $\Delta V(\mathrm{H\,II\text{-}CO}) = -3.4 \pm 0.4$ km s^{-1}, while the obscured H II regions do not show such an effect: $\Delta V(\mathrm{H\,II\text{-}CO}) = -0.5 \pm 0.4$ km s^{-1}. This result confirms an essential property of the blister model, namely that ionized gas streams away from the associated CO clouds. Two comments must be made at this stage.

Firstly, the blue-shift of visible H II regions is on average surprisingly small. Again assuming that the CO clouds are spherical, and that the orientation of the H II region on the CO cloud is random, I would expect a velocity difference between 0.5 and 1.5 times the speed of sound. For a sound speed of 10 km s^{-1}, we then get a value more than twice the observed value. This discrepancy may be caused by several factors: there may be large errors in some velocity determinations, geometrical effects such as CO cloud shapes differ strongly from spheres, preferential orientations H II regions/CO clouds with respect the Sun; or the bulk of the ionized material may still be somewhat contained in the cavity. The first two possibilities might apply to the presence of five optically visible H II regions with "forbidden" redshifts larger than +2.5 km s^{-1}. Certainly S 142, whose H II region is larger than the CO cloud and which appears to show a redshift of +5.2 km s^{-1}, is a case in point. It is difficult to estimate the effect of the last possibility, but it will certainly play a role. More observations of higher quality are needed.

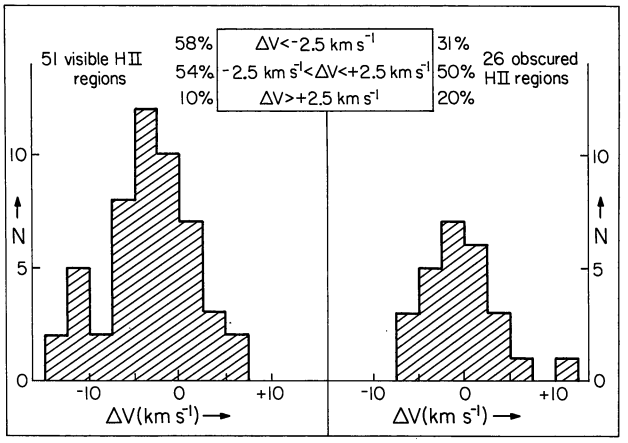

Fig. 3. Distribution of the velocity difference ΔV (H II-CO) for visible and for obscured H II regions

Secondly, while most of the optically visible H II regions are in nearby parts of the Galaxy (Perseus Arm, Local Spiral Arm), most of the obscured H II regions are in the inner, more distant parts of the Galaxy, obscured by dust clouds in one or more intervening spiral arms. Thus, as mentioned above, the zero result for these regions, rather than an expected positive bias (redshift), is not surprising and does not argue against the general applicability of the blister model.

VII. Conclusion

In summary, I conclude that H II regions appear to form at the edges of CO clouds that have typical diameters of 5–10 pc. They show ionization fronts eating into the associated neutral clouds, with diffuse gas streaming away from the fronts. The average line-of-sight velocity difference between an H II region and its CO cloud is about 3 km s^{-1}. Although further case studies are desirable, it appears that the blister model is an excellent working hypothesis for the interpretation of H II region structure in general.

As a consequence, the origin and evolution of an H II region should be regarded as part of the development of a larger, more massive neutral cloud or cloud complex. More specifically, models of the structure and evolution of H II regions should take into account the extremely asymmetric pressure and density conditions (which result from the fact that one part of the H II region interfaces with a neutral cloud), rather than assume spherical symmetry. Moreover, the apparent general applicability of the blister model, with its concomitant notion that massive stars tend to form at the edges of neutral clouds, has important consequences for theories of star formation.

Table 3. Radial Velocities of H II Regions and Associated CO Clouds

Name		$V_{H109\alpha}$ (km s^{-1})	$V_{H\alpha}$ (km s^{-1})	V_{CO} (km s^{-1})	ΔV_{HII-CO} (km s^{-1})	ℓ	b	Remarks	Ref.
W28S		+10.5±0.6	-	+8±1.5	+2.5±1.6	5.9	-0.4	Obscured	1,2
S25	W29;M8;NGC6523	+3.0±0.3	+5.7±2.0	-10±1.5	-7.0±1.5	6.0	-1.2		1,2,3,4
W28N		+14.2±0.7	-	+19±1.5	-4.8±1.7	6.6	-0.1	Obscured	1,2
S30	M20;NGC6514	+16.4±1.8	+11.3±2.0	+18±1.5	-1.6±2.3	7.0	-0.2		1,2,3
W31		+9.7±1.1	-	+12±1.5	-2.3±1.9	10.3	-0.1	Obscured	1,2,4
W33		+36.3±0.4	-	+35±1.5	+1.3±1.6	12.8	-0.2	Obscured	1,2
		+0.3±1.2	-	-3±1.5	+3.3±1.9	10.6	-0.4	Obscured	1,2
S45	M17;NGC6618	+17.2±0.2	+19 ±2.0	+22±1.5	-4.8±1.5	15.1	-0.7		1,2,3,4
S48		-	+36.0±2.0	+46.3±1.0	(-9.7±2.2)	16.7	-0.3		3.5
S49	M16;NGC661	+24.5±0.6	+28.4±2.0	+23±1.5	+1.5±1.6	17.0	+0.8		1,2,3,4
W41		+82.5±4.0	-	+72±1.5	+10.5±4.3	22.8	-0.3	Obscured	1,2
S57		-	+24.0±2.0	+36.6±1.0	(-12.6±2.2)	22.9	+0.7		3,5
W40		+0.7±1.3	-	+6±1.5	-5.3±2.0	28,8	+3.5	Obscured	1,2
W43		+92.3±0.3	-	+97±1.5	-4.7±1.5	30.8	+0.0	Obscured	1,2,4
		+99.2±2.0	-	+101±1.5	-1.8±2.5	31.1	+0.0	Obscured	1,2,4
S69		-	+49.5±2.0	+55.4±0.7	(-5.9±2.1)	32.0	+1.2		3,6
W44		+53.9±0.7	-	+55±1.5	-1.1±1.7	34.3	0.1	Obscured	1,2
W48		+46.5±2.4	-	+42±1.5	+4.5±2.8	35.2	-1.7	Obscured	1,2
W49		+8.6±0.6	-	+10±1.5	-1.4±1.6	43.2	-0.0	Obscured	1,2,4
G45.5+0.1		+53.0	-	+56.6	-3.6	45.5	+0.1	Obscured	7,8
G45.5+0.0		+57.0	-	+57.2	-0.2	45.5	+0.0	Obscured	7,8
W51		+63.2±1.2	-	+70±1.5	-6.8±1.9	49.0	-0.3	Obscured	1,2,4
		+67.2±1.4	-	+68±1.5	-0.8±2.1	49.2	-0.3	Obscured	1,2
S82		-	+14.6±2.0	+24.5±1.0	(-9.9±2.2)	53.6	+0.0		3,5
S84		-	+27.2±2.0	+28.3±1.0	(-1.3±2.2)	55.8	-3.8		3,5
S88		-	+17.6±2.0	+22.9±0.7	(-5.3±2.1)	61.3	+0.5		3,6
S90		+15.3±2.8	+22.5±2.0	+22.2±0.7	-6.9±2.9	63.2	+0.5		1,3,6
S93		+23.1±0.5	-	+21.3±0.7	+1.8±0.8	74.2	-0.5		9,6
S99		-	-22.0±2.0	-22.9±0.7	(+0.9±2.1)	70.1	+1.7		3,6
S100	(W58;NGC6857)	-24.4±0.8	-21.7±2.0	-24±1.5	-0.4±1.7	70.3	+1.6		1,2,3
S104		0±4	-0.4±2.0	+2.8±1.0	-2.8±4.1	74.8	+0.6		5,6,10
ON2		-4.8	-	+1.2	-6.0	75.8	+0.6	Obscured	2,8
DR22		-1.0±0.9	-	-1±1.5	0±1.8	80.9	-0.2	Obscured	1,2
DR17		+11.3±0.6	-	+9±1.5	+2.3±1.6	81.4	+1.2	Obscured	1,2
DR23		+0.2±0.9	-	-6±1.5	+6.2±1.8	81.6	+0.0	Obscured	1,2
DR21	(W75S)	+1.7±0.5	-	-2±1.5	+3.7±1.6	81.7	+0.5	Obscured	1,2
W75N		+6		+11	-5	81.9	+0.8	Obscured	1,21
S112		-	-9.7±2.0	-12.1	(+2.4±2.2)	83.7	+3.1		3,5
S117	(NGC7000)	-	+3.0±2.0	+4.4	(-1.4)	85.0	-1.0		3,11
S125	(IC5146)	-	+4.8±2.0	+7.6	(-2.8)	94.3	-5.5		3,11
S128		-	-69.2±2.0	-74.0±1.0	(+4.8±2.2)	97.5	+3.1		3,5
S135		-	-17.6±2.0	-20.8±0.7	(+3.2±2.2)	104.6	+1.2		3,6
S139		-	-17.6±2.0	-15.0±1.0	(-2.6±2.2)	105.8	+0.0		3,5
S140		-	-10.0±2.0	-8.0±0.7	(-2.0±2.2)	106.8	+5.3		3,6
S142		-	-35.8±2.0	-41.0±1.0	(+5.2±2.2)	107.1	-0.9		3,5
S144		-	-1.7±2.0	-6.7±1.0	(-8.4±2.2)	107.3	+0.9		3,5
S146		-56.9±0.5	-	+49.5±0.7	-7.4±0.8	108.2	+0.6		6,9
S152		-50.4±0.5	+62.2±2.0	-51 ±0.7	+0.6±0.8	108.8	-1.0		3,9,12
S155		-	-15.1±2.0	-12.3±0.7	(-2.8±2.5)	110.2	+2.6		3,13
S156	(IC1470)	-64.7±0.5	-50.0±2.0	-52 ±0.7	-12.7±0.8	110.1	+0.0		3,9,12
S157A		-	-46 ±2.0	-42.8±1.0	(-2.1±2.1)	111.1	-0.7		12,14
S158	(NGC7538)	-60.6±0.8	-59.6±2.0	-55 ±1.5	-5.6±1.7	111.6	+0.9		1,2,3
S168		-	-43.5±2.0	-39.6±0.7	(-3.9±2.1	115.8	-1.6		3,6
S171	(W1;NGC7822)	-	-12.8±2.0	-12 ±1.5	(-0.8±2.5	118.5	+6.0		1,3
W3A		-40	-	-41 ±1.5	-1	133.7	+1.2	Obscured	1,15
W3B		-35	-	-40 ±1.5	-5	133.7	+1.2	Obscured	1,15
W3OH		-49	-	-47 ±1.5	+2	133.9	+1.1	Obscured	1,15
S199	(IC1848)	-37.6±5.4	-36.9±0.7	-38.9±0.7	+1.3±5.5	137.6	+1.2		3,11,16
S206	(NGC1491)	-26.3±0.8	-26.5±1.0	-22.2±0.7	+4.1±1.1	150.6	-0.9		1,4,17
S219		-	-24.9±2.0	-23.5±0.7	(-1.4±2.1)	159.3	+2.6		3,6
S228		-	-12.0±2.0	- 8.3±0.7	(-3.7±2.9)	169.2	-1.0		3,12
S235		-24.6±0.5	-24.5±2.0	-20.5±0.7	-4.1±0.8	173.5	+2.7		3,6,9
S252	(NGC2175)	-	+6.9±2.0	+8 ±2.5	-1.1±3.0	190.0	+0.5		3,18
S255	(IC2162)	+6.0±0.5	+5.3±2.0	+7.8±0.7	-1.8±0.8	192.5	+0.1		3,6,9
S269		+10.9±0.5	+13.6±2.0	+17.5±0.7	-6.6±0.8	196.4	-1.7		1,3,6,9
S273	(NGC2264)	-	+1,9±2.0	+8 ±1.5	(-6.1±2.5)	203.0	+2.0		1,3
OriB	(W12;NGC2024)	+7 ±0.2	-3.5±2.0	+11 ±1.5	-4.0±1.6	206.5	-1.6		1,2,3
S281	(OriA;W111,NGC1976)	-2.7±0.5	-	+9 ±1.5	-11.7±1.6	209.0	-1.9		1,2
S294		-	+35.2±2.0	+32.5±0.7	(+2.7±2.1)	224.2	+1.2		3,6
S297		-	+7.8±2.0	+11.7±0.7	(-3.9±2.1)	225.5	-2.6		3,6
S307		-	+34.9±2.0	+45.6±0.7	(-10.9±2.1)	234.8	-0.2		3,6
S309		-	+31.9±2.0	+42.8±0.7	(-10.7±2.1)	234.5	+0.8		3,6
S10		-	+13.8±2.0	+24 ±1.0	(-10.2±2.1)	239.1	-5.2		3,19
MSH1730-33		-12.3±0.5	-	-13 ±1.5	+0.7±1.6	348.7	-1.0	Obscured	1,2
NGC6334		-2.5±0.3	-7.0±2.0	-8 ±1.5	+6.5±1.5	351.2	+0.7		1,2,3
W22	(NGC6357)	-2.9±0.4	-6.6±2.0	-3 ±1.5	+0.1±1.6	253.1	+0.7		1,2,3,4
H2-3		-21.1	-23.5	-21 ±1.5	-0.1	354.4	-0.9		1,7,20

1. Wilson et al. (1974)
2. Refenstein et al. (1970)
3. Georgelin (1975); Georgelin et al. (1973)
4. Mezger and Höglund (1967)
5. This Paper
6. Blair et al. (1975)
7. Caswell
8. Baud (1977)
9. Kazès et al. (1977)
10. Dickel and Milne (1972)
11. Milman et al. (1975)
12. Dickinson et al. (1974)
13. Sargent (1977)
14. Deharveng (1974)
15. Wellington et al. (1976)
16. Hart and Pedlar (1976)
17. Walmsley et al. (1975)
18. Baran, private communication
19. Lada and Reid (1977)
20. Rubin and Turner (1971)
21. Morris et al. (1974)

Acknowledgement. It is a pleasure to thank Harm Habing, Vincent Icke, Jill Knapp and Anneila Sargent for comments. I am particularly indebted to Pat Thaddeus for giving me part of his observing time at the Texas Millimeter Wave Observatory, and to Leo Blitz and Hong-ih Cong for introducing me to the telescope and helping with the observations.

Part of this work was supported by the National Science Foundation grant MPS73-04677.

References

Balick, B., Gammon, R. M., Hjellming, R. M.: 1974, in H II *Regions and the Galactic Center,* ed. by A. F. M. Moorwood, 8th SLAB Symposium, ESRO SP-105, p. 28
Baud, B.: 1977, *Astron. Astrophys.* **57**, 443
Blair, G. N., Peters, W. L., Van den Bout, P. Q.: 1975, *Astrophys. J. Letters* **200**, L161
Blair, G. N., Evans, N. J., Van den Bout, P. A., Peters, W. L.: 1977, *Astrophys. J.* (in press)
Caswell, J. L.: 1968, *Astron. J.* **73**, 949
Deharveng, L.: 1974, *Astron. Astrophys.* **35**, 63
Deharveng, L.: 1973, *Astron. Astrophys.* **29**, 341
Deharveng, L., Israel, F. P., Maucherat, M.: 1976, *Astron. Astrophys.* **48**, 63
Dickel, J. R., Milne, D. K.: 1972, *Australian J. Phys.* **25**, 539
Dickinson, D. F., Frogel, J. A., Persson, S. E.: 1974, *Astrophys. J.* **192**, 347
Dopita, M. A., Dyson, J. E., Meaburn, J.: 1974, *Astrophys. Space Sci.* **28**, 61
Dopita, M. A., Isobe, S., Meaburn, J.: 1975, *Astrophys. Space Sci.* **34**, 91
Dyson, J. E.: 1973, *Astron. Astrophys.* **27**, 459
Dyson, J. E.: 1977a, *Astron. Astrophys.* **59**, 161
Dyson, J. E.: 1977b, *Astron. Space Sci.* **51**, 197
Elliott, K. H., Meaburn, J.: 1974a, *Astron. Astrophys.* **34**, 473
Elliott, K. H., Meaburn, J.: 1974b, *Astrophys. Space Sci.* **28**, 351
Elliott, K. H., Meaburn, J.: 1975a, *Astrophys. Space Sci.* **35**, 81
Elliott, K. H., Meaburn, J.: 1975b, *Monthly Notices Roy. Astron. Soc.* 1972, 427
Elliott, K. H., Goudis, C., Meaburn, J., Tebbutt, W. J.: 1977, *Astron. Astrophys.* **55**, 187
Felli, M., Habing, H. J., Israel, F. P.: 1977, *Astron. Astrophys.* **59**, 43 (Paper V)
Georgelin, Y. M.: 1975, Ph. D. thesis Universite de Provence, Marseille (France)
Georgelin, Y. P., Georgelin, Y. M., Roux, S.: 1973, *Astron. Astrophys.* **25**, 337
Goudis, C., Meaburn, J.: 1974, *Astron. Astrophys.* **34**, 437
Goudis, C., Meaburn, J.: 1976, *Astron. Astrophys.* **51**, 401
Gull, T. R., Belich, B.: 1974, *Astrophys. J.* **192**, 63
Hart, L., Pedlar, A.: 1976, *Monthly Notices Roy. Astron. Soc.* **176**, 135
Harten, R. H.: 1976, *Astron. Astrophys.* **46**, 109
Icke, V.: 1973, *Astron. Astrophys.* **26**, 45
Israel, F. P.: 1976a, *Astron. Astrophys.* **48**, 193 (Paper II)
Israel, R. P.: 1976b, *Astron. Astrophys.* **52**, 175 (Paper III)
Israel, F. P.: 1977a, *Astron. Astrophys.* **59**, 27 (Paper IV)
Israel, F. P.: 1977b, *Astron. Astrophys.* **60**, 233 (Paper VI)
Israel, F. P., Habing, H. J., de Jong, T.: 1973, *Astron. Astrophys.* **27**, 143 (Paper I)
Israel, F. P., Felli, M.: 1977, *Astron. Astrophys.* **63**, 325
Kazès, I., Walmsley, L. M., Churchwell, E.: 1977, *Astron. Astrophys.* 60, 293
Lada, L. J., Reid, M. J.: 1978, *Astrophys. J.* (in press)
Liszt, H. T.: 1973, Ph. D. thesis, Princeton University (USA)
Lucas, R., Encrenaz, P. J.: 1975, *Astron. Astrophys.* **41**, 233
Lynds, B. T.: 1965, *Astrophys. J. Suppl.* **13**, 163
Martin, A. H. M., Gull, S. F.: 1975, *Monthly Notices Roy. Astron. Soc.* **75**, 235
Mathews, H. E., Goss, W. M., Winnberg, A., Hebing, H. J.: 1977, *Astron. Astrophys.* **61**, 261
Meaburn, J.: 1975a, *Astrophys. Space Sci.,* **35**, L5
Meaburn, J.: 1975b, in H II *Regions and Related Topics,* ed. by T. L. Wilson and D. Downes, Springer, Heidelberg (BRO), p. 222
Meaburn, J.: 1977 in *Topics in Interstellar Matter,* ed. by H. van Woerden, Reidel Publ. Co., Dordrecht (Netherlands), p. 81
Mezger, P. G., Höglund, B.: 1967, *Astrophys. J.* **147**, 490
Milman, A. S., Knapp, G. R., Wilson, W. J.: 1975, *Astron. J.* **80**, 101
Morris, M., Palmer, P., Turner, B. E., Zuckerman, B.: 1974, *Astrophys. J.* **191**, 349
Reifenstein, E. C., Wilson, T. L., Burke, B. F., Mezger, P. G., Altenhoff, W. J.: 1970, *Astron. Astrophys.* **4**, 357
Rubin, R. H., Turner, B. E.: 1971, *Astrophys. J.* **165**, 471
Sargent, A. I.: 1977, Ph. D. thesis, Calif. Inst. Techn., Pasadena, Calif., (USA)
Tenorio-Tagle, G.: 1977, *Astron. Astrophys.* **54**, 517
Walmsley, C. M., Churchwell, E., Kazès, I., Le Squéren, A. H.: 1975, *Astron. Astrophys.* **41**, 121
Wellington, K. J., Sullivan, W. T., Goss, W. M., Mathews, H. E.: 1976, *Astron. Astrophys.* **47**, 351
Wilson, O. C., Munch, G., Flather, E. M., Coffeen, M. F.: 1959, *Astrophys. J. Suppl.* **4**, 199
Wilson, W. J., Schwartz, P. R., Epstein, E. E., Johnson, W. A., Etcheverry, R. D., Mori, T. T., Berry, G. G., Dyson, H. B.: 1974, *Astrophys. J.* **191**, 357
Zuckerman, B.: 1973, *Astrophys. J.* **183**, 863